Sub-15nm Optical Fiber Nanoimprint Lithography: A Parallel, Self-aligned and Portable Approach

Gorgi Kostovski, Udayakumar Chinnasamy, Sasani Jayawardhana, Paul R. Stoddart, and Arnan Mitchell*

Advances in nanoscale fabrication provide access to the small-scale phenomena that underpin fields of research such as plasmonics and subwavelength optics.[1] The choice of substrate for these nanostructures can define the scope of their utility. Nanostructures on an optical-fiber facet obtain the advantages of a miniaturized substrate that can be interrogated remotely and deployed in vivo and in vitro. However, fabrication on fiber facets is challenging, because of their unusually small 125 μm diameter and their large aspect ratio. To date, demonstrations of fiber-facet nanopatterning have used interference lithography (IL),[2] electron-beam lithography (EBL)[3–5] and focused ion-beam lithography (FIB)[6,7] as fabrication techniques. The transfer of EBL nanostructures to fiber facets has also been demonstrated,[8,9] achieving 25 nm feature separations. However, IL can produce only limited geometries, while EBL and FIB are unsuited to high-throughput fabrication.

In contrast, nanoimprint lithography (NIL) provides large-area, high-resolution nanofabrication at low cost and high-throughput. New platforms that have been explored for NIL include mask aligners,[10] roll-to-roll imprinting,[11] optical-fiber lengths[12] and optical-fiber-facets (OFF-NIL). To date, OFF-NIL has demonstrated periodic diffraction features with dimensions 250 nm,[13] and 630 nm,[14,15] and nanorods for surface-enhanced Raman scattering (SERS) with diameters ~110 nm.[16]

All of these demonstrations of fiber-facet nanopatterning have been limited to single-fiber processing. Given the typical facet diameter of 125 μm, there is clear opportunity for increased throughput via parallel OFF-NIL with large-area molds. Fiber-ribbons would seem an appropriate candidate for parallel fabrication,[17] however these are restricted in the type and number of fibers available, and require specialized stripping and cleaving tools. Additionally, the cleaved ribbon-facets are restricted to a single plane.

In this paper, we demonstrate an elegant, low-cost, highly accessible platform for imprinting arrays of optical-fiber facets. We show that by segmenting optical-fibers into short lengths and loading them into separate U-grooves, many fibers can be imprinted in parallel. Over-sizing these U-grooves enables the fibers to independently slide back-and-forth, and to self-align once they contact the mold, eliminating the need for critical proximity control during imprinting. Using this platform, we have achieved sub-15 nm feature separations across fiber arrays. Further, using this system with large-area molds eliminates the need for critical lateral alignment. The demands on the imprinting platform are thus reduced to providing coarse, uniaxial translation, allowing us to demonstrate a compact, portable module for fiber-array imprinting. Finally, self-alignment uniquely accommodates non-planar molds, allowing us to employ a biological nanotemplate.

Arrays of optical-fibers were created using arrays of U-grooves, shown in **Figure 1**. Their width and depth were set to 150 μm, marginally exceeding the 125 μm fiber diameter. This 25 μm leeway allowed the fibers to slide freely within the channels, as illustrated in **Figure 2**. Channel separation was 150 μm, to prevent polymer from bridging adjacent facets. For demonstration purposes, short 25 mm lengths of silica fiber were manually loaded into these U-grooves.

Two large-area molds were used for this work. The first was the highly planar, self-assembled nanostructure of anodized aluminum oxide (AAO). This allowed us to produce sub-15 nm features[18–20] with which to establish the resolution of this array imprinting process. An ultrathin PDMS antiadhesion layer[18] was added to this mold. The second mold was cast from the antireflective nanostructure on a cicada wing (*Platylomia radah*), into the low surface-energy elastomer h-PDMS.[16,21] The non-planarity of this wing was used to demonstrate self-aligned array imprinting. The cicada wing nanostructure consists of a 2D array of pillars, with period ~200 nm, height ~300 nm, and apex width ~70 nm. Both molds were transparent to visible and UV light and offered centimeters of surface area.

Two platforms were used for imprinting with the U-grooves. The first was a vibration isolated optical-fiber autoalign system (Newport, AAMODAL). This was used with the <15 nm AAO mold. The second was a much simpler, manual, linear-translation stage (Parker Daedal). This had a footprint of 6 cm × 13 cm, small enough to serve as a portable imprinting module. The non-planar cicada mold was used here. The large area of this mold required no lateral alignment of the fibers, complementing the uniaxial motion offered by the translation stage. This stage was adapted to imprinting by adding one component for holding the U-grooves, and a second for holding the NIL mold. These were machined from aluminum and attached using pre-existing threaded holes to form a mechanically stable device.

Dr. G. Kostovski, U. Chinnasamy, Prof. A. Mitchell
Platform Technologies Research Institute
Microplatforms Research Group
School of Electrical and Computer Engineering
RMIT University,
Melbourne, Victoria 3001, Australia
E-mail: gorgi.kostovski@rmit.edu.au
S. Jayawardhana, Dr. P. R. Stoddart
Faculty of Engineering and Industrial Science
Swinburne University of Technology
Hawthorn, VIC 3122, Australia

DOI: 10.1002/adma.201002796

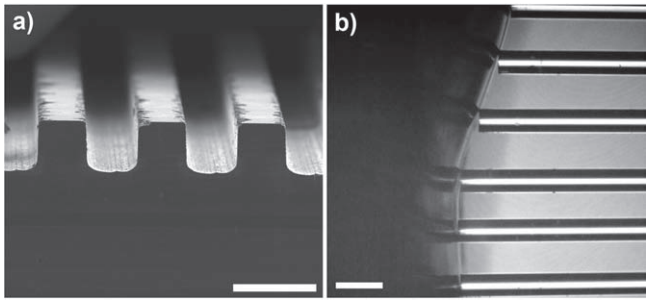

Figure 1. SEM image of a) diced U-grooves and b) photograph of the fiber-array self-aligning against the cicada mold. Scale bars are both 250 µm.

The negative photoresist SU8-2002 (Microchem) was employed for imprinting the fiber facets. This was manually dispensed by syringe, and the volume was only coarsely monitored. Imprinting against the cicada mold required a greater volume to accommodate its nonplanarity.

The critical role of self-alignment during imprinting is shown in Figure 1B, where the non-planar cicada mold has offset adjacent facets by >50 µm. On the portable module, self-alignment was performed entirely in-hand, independent of magnification optics or vibration isolation. It is expected that the relaxed confinement of the light-weight and flexible fibers could accommodate some mechanical vibration, reducing its impact at the polymer/mold interface. However in translating forward, the free length of fiber between U-grooves and mold was minimized to maximize fiber stability.

After self-aligning, a thermal treatment was applied to dissipate solvents from the SU8 and induce reflow. This allowed the mold nanofeatures to be filled by capillary forces rather than requiring high pressures, which may have conflicted with the axial freedom of the fibers. On the autoalign system, a constant temperature was maintained by a resistive heating element to minimize thermal stress. However, the portable module was heated by placing it inside a convection oven, emphasizing its portability. The module was briefly removed from the oven for a UV exposure through the mold, after which it was returned to the oven for post-baking.

After curing the imprinted polymer, the fibers were immobilized within their U-grooves using polyimide adhesive-tape, which exhibits low residue and high temperature stability. The fibers were then separated from the mold. The polyimide tape then served its second function of unloading the fibers from the U-grooves while preserving their ordered arrangement, by simply peeling it away, as illustrated in Figure 2. The imprinted fibers could then be stored while attached to this tape, with individuals peeled away as required.

Despite the PDMS anti-adhesion layer, we encountered difficulty with releasing cured SU8 from the AAO mold, resulting in mold contamination. Yield was improved by careful control of the UV dose, and the addition to the fiber facet of an intermediate SU8 layer[22], which was intentionally overexposed for firm adhesion. In contrast, separating from the h-PDMS cicada mold presented little difficulty. We attribute this difference to their contrasting surface-area and mechanical flexibility. On the autoalign platform, we were able to successfully imprint ten optical-fibers in parallel against the AAO mold, while the full U-groove capacity of 40 fibers was imprinted with the portable module against the cicada mold.

Both imprinting platforms produced high fidelity replicas of their respective molds. The AAO template in **Figure 3A** is in clear agreement with the AAO imprints in Figure 3B, which has feature separations that are <15 nm. Similarly, the cicada wing template shown in Figure 3C is in agreement with the facet replica in Figure 3D. This fidelity was consistent across the entire array of 10 fibers for the AAO patterns, and 40 fibers for the cicada patterns. While the elevated temperatures used for curing the polymer suggest that some thermal shrinkage may be present in the replicated patterns, this was difficult to identify, since both patterns were semi-random in nature.

Central to self-alignment is the physical contact made between facets and molds, and the resistance offered by the U-grooves. The force exerted by each facet while actively winding forward was ~60 mN, for a 25 mm long fiber in a 20 mm long U-groove. The non-planarity of the flexible cicada mold thus occasionally subjects it to a slight compression by facet edges, as in Figure 1B. SEM examination revealed this compression to be localized to within ~5 um of the facet edge, and was generally quite mild, such that replicated nanofeatures were continuous over the facet edge. This same compression was not apparent in the AAO imprints. It is expected that this contact force could be minimized by reducing the contact area between U-groove and fiber.

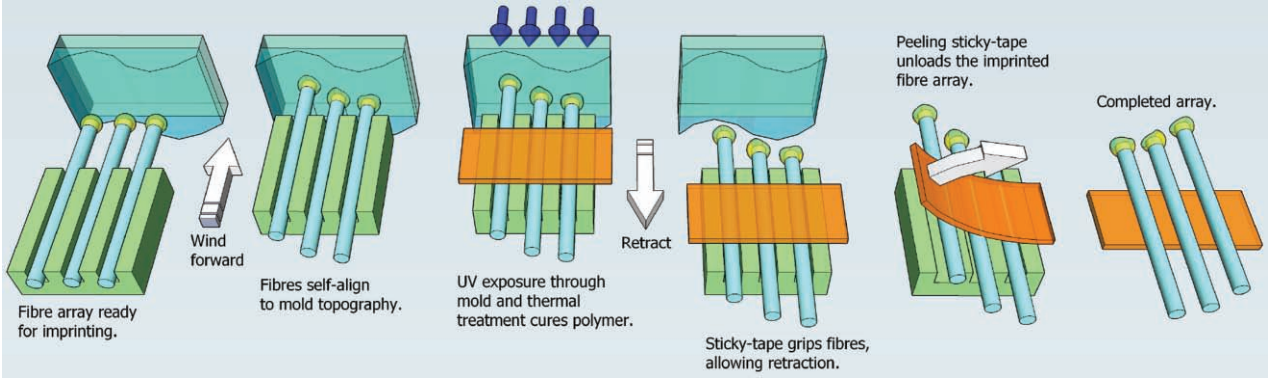

Figure 2. Process diagram illustrating the self-aligned, array-imprinting sequence against a non-planar, large-area mold.

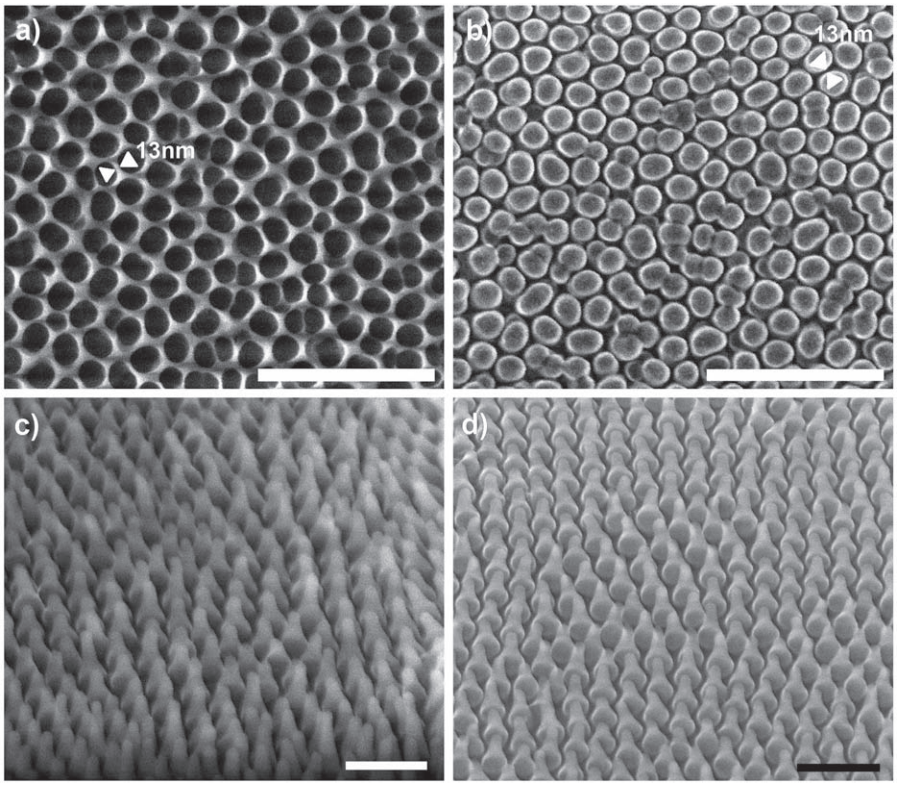

Figure 3. SEM images of a) the AAO mold, b) the imprinted AAO structure on the fiber-facet, c) the cicada wing template and d) the SU8 replica on a fiber facet. Scale bars are all 500 nm.

The total time to imprint 40 fibers with the portable module and cicada mold was about 2 h, or 3 min/fiber. The dominant time factors were the two 30 min bakes, and the ~30 min for fiber cleaving and loading. Imprinting 10 fibers with the AAO mold and autoalign platform took ~90 min, due to dual SU8 layers and numerous system alignments. Future work could improve throughput by using a UV curable polymer, which would allow room-temperature imprinting,[10–12] and by automating fiber cleaving and loading. Alternatively, due to the modular nature of the portable imprint tool, these 30-minute processes could be conducted on multiple modules, in a pipeline process.

While the portable imprint module is not a truly self contained imprinting platform, the external components that it depends on are common to most research labs. To summarize, these consist of an optical-fiber cleaver, a convection oven, and a UV source. This compatibility with existing infrastructure makes this platform widely useful at low cost.

To demonstrate an application of these nanostructured facets, they were made plasmonically active with a thin silver coating and employed for SERS sensing.[16,23–26] SERS provided a quantitative optical method for validating the pattern integrity of the facets and offers important potential applications.[24] Preparation was completed by coating the probes with a self-assembled monolayer of thiophenol, a common SERS analyte.[25–27] Their bi-directional functionality was then tested by taking two SERS measurements, first by direct interrogation of the nanostructured facet, then in the through-fiber optrode configuration, where the fiber core carries both the excitation and scattered light. **Figure 4A** shows five representative SERS spectra, consisting of direct and through-fiber measurements of cicada and AAO imprinted fibers, and a cicada wing reference spectrum. Distinct thiophenol peaks are present in all fiber measurements, and through-fiber spectra show reasonable signal-to-noise ratio, despite additional losses associated with the optrode geometry. The superior performance of the chitin cicada reference relative to the SU8 replica is attributed to larger clustering in its Ag coating morphology.

These same measurements were repeated for the 40 optical-fibers imprinted with the cicada pattern, and the 10 fibers imprinted with the AAO pattern. A set of 40 measurements from across a cicada wing were also acquired for reference. The resulting set of 140 spectra is presented in Figure 4B, where each spectrum is represented by a single data-point. Figure 4B verifies the consistent SERS performance of each fiber in the two imprinted arrays, in both direct and through-fiber interrogation. By extension, this verifies the successful patterning of the fiber arrays with our two nanotemplates, and thus the validity of our self-aligned, portable, array-imprinting technique.

In closing, we have taken the first steps toward a general platform for imprinting arrays of optical-fiber facets with 2D polymer nanostructures. The technique is simple, low-cost and inherently self-aligning, providing access to both planar and non-planar molds alike, on both highly-engineered systems and portable imprint modules. We have demonstrated a capacity for 40-fiber imprinting against nonplanar molds with 70 nm features, and 10-fiber imprinting with <15 nm feature separations. We performed chemical detection with these 50 imprinted

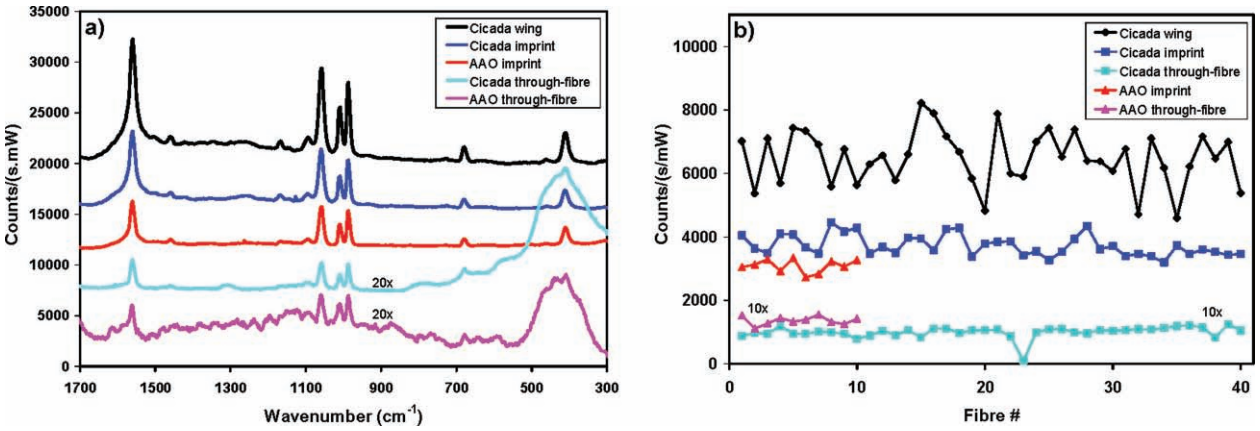

Figure 4. Representative thiophenol SERS spectra are shown in a). Spectra have been vertically offset for clarity. Array data is shown in b).

fibers to demonstrate their functionality as bi-directional SERS probes, and to verify consistent nanopatterning. Future work will explore further opportunities for improving both throughput and resolution.

Experimental Section

Fabrication and loading of fiber-arrays: U-grooves were cut into Si wafers with a dicing saw (Disco DAD 321, NBC-ZB-1120 blade). Width, depth and separation were all 150 µm. Multimode silica optical-fibers (Corning 62.5/125 0.272 NA) were prepared by stripping their jackets, wiping with methanol, cleaving into 25 mm lengths and loading into U-grooves with tweezers.

Fabrication of AAO sub-15nm mold: A 1.2 µm film of Al (Strem Chemicals, 5N) was deposited by e-beam evaporation (EBE) onto a glass slide. This was annodized at 40 V in 0.3 M $C_2H_2O_4$ using a two step process to improve pore ordering. The first anodization lasted ~9 min, consuming the top ~1 µm of Al. This was stripped away in a solution of 1.8wt% CrO_3 and 6wt% H_3PO_4 at 65 °C for 45 min. The remaining Al was then completely anodized. Afterwards, pores were widened in a 5wt% H_3PO_4 solution for >1 hour until wall thickness was <15 nm and pore diameter was ~80 nm. Aspect ratio was ~1:1. The nanopore distribution was semi-random due to the limited Al thickness available from EBE.

Fabrication of the cicada mold: These were cast in a mixture of h-PDMS and hexane[16,21] and backed with a glass slide.

Imprinting with the AAO mold and auto-aligner: The U-groove array was loaded onto an xyzθ translation stage, while the mold was loaded opposite onto a rigid aluminum mount. The fiber facets were loaded with polymer and self-aligned against the mold. Thermal treatment was performed by convection from a resistive heating element below the fibers. A 7 min thermal ramp prevented thermal shocking of the mold and reflowed the SU8, filling the mold nanofeatures by capillary forces. The temperature was kept constant for the duration of the imprinting to minimize thermal stresses. A 10 s ultraviolet exposure (EXFO Novacure spot-curing), directed through the mold, initiated cross-linking of the epoxy, and was followed by a 1 min post-bake. Polyimide tape (Associated Gaskets Pty Ltd) was applied to grip the fibers and they were separated from the mold.

Imprinting with the cicada mold and the portable imprinter: Initial bake was performed in a convection oven at 125 °C for 30 min, after which the portable module was removed from the oven for a 10 s UV exposure. Total time outside the oven was <1 min, minimizing thermal shrinkage. A further 30 min at 125 °C achieved post-exposure cross-linking. Polyimide-tape was then applied to the U-grooves, while still inside the oven, allowing fiber separation from the mold.

SERS testing: Imprinted facets were metallized with 60 nm Ag (Aldrich, 6N) by thermal evaporation (Emitech K975X) at normal incidence, under rotation. These were then immersed for 10 min in a test analyte solution of 10 mM thiophenol in ethanol,[25–27] allowing the thiophenol to adsorb on the Ag surface. Excess thiophenol was rinsed away with ethanol, and the fibers were air dried prior to SERS testing.

The bi-directional functionality of each fiber was tested with a modular Raman microscope (Horiba-Yobin Yvon), Triax 320 spectrometer, and thermoelectrically cooled CCD (Horiba-Yobin Yvon), using a 532 nm excitation wavelength (OptoTech Ltd. Melbourne) and a 50× objective lens (0.5NA). Direct interrogation of the imprinted facets used 0.29 mW of optical power, a 3 s acquisition and 5 averages. In contrast, through-fiber interrogation introduces a Raman contribution from the fiber itself, while also reducing the power density at the nanostructured facet. Numerical aperture mismatch between fiber and objective lens also reduces signal level. Thus, a longer 5 s acquisition time was used for through-fiber measurements of the cicada imprints, while 10 s was necessary for the AAO fibers. A power of 1.33 mW at the objective was used for both through-fiber sets. Post acquisition processing was limited to a linear slope correction on the AAO through-fiber spectrum, for presentability. The broad peaks at 420 cm^{-1} in the through-fiber spectra are background silica peaks generated by Raman scattering from the fiber core. For the representation of array data, from each of the 140 spectra, the average height was taken of the three central thiophenol peaks at 1072, 1021, and 1000 cm^{-1}, after correcting for baseline slope, and this average was scaled to counts s^{-1} mW^{-1} to produce the plotted data points.

Supporting Information

Supporting Information is available from the Wiley Online Library or from the author.

Acknowledgements

The authors thank the NHMRC for Development Grant No. 499321, the RMIT Microscopy and Microanalysis Facility, and Yuxun Cao, Vijay Sivan and Robert Kealy for technical assistance.

Received: August 3, 2010
Published online: November 22, 2010

[1] K. Busch, G. v. Freymann, S. Linden, S. F. Mingaleev, L. Tkeshelashvili, M. Wegener, *Phys. Rep.* **2007**, *444*, 101.
[2] S. Feng, X. Zhang, H. Wang, M. Xin, Z. Lu, *Appl. Phys. Lett.* **2010**, *96*, 133101.
[3] E. J. Smythe, E. Cubukcu, F. Capasso, *Opt. Express* **2007**, *15*, 7439.
[4] Y. Lin, J. Guo, R. G. Lindquist, *Opt. Express* **2009**, *17*, 17849.

[5] L. Tian, S. Frisbie, A. A. Bernussi, M. Holtz, *J. Appl. Phys.* **2007**, *101*, 014303.
[6] A. Dhawan, J. F. Muth, *Mater. Sci. Eng. B* **2008**, *149*, 237.
[7] A. Dhawan, M. Gerhold, A. Madison, J. Fowlkes, P. E. Russell, T. Vo-Dinh, D. N. Leonard, *Scanning* **2009**, *31*, 139.
[8] E. J. Smythe, M. D. Dickey, G. M. Whitesides, F. Capasso, *ACS Nano* **2009**, *3*, 59.
[9] E. J. Smythe, M. D. Dickey, J. Bao, G. M. Whitesides, F. Capasso, *Nano Lett.* **2009**, *9*, 1132.
[10] W. Wu, W. M. Tong, J. Bartman, Y. Chen, R. Walmsley, Z. Yu, Q. Xia, I. Park, C. Picciotto, J. Gao, S-Y. Wang, D. Morecroft, J. Yang, K. K. Berggren, R. S. Williams, *Nano Lett.* **2008**, *8*, 3865.
[11] S. H. Ahn, L. J. Guo, *Adv. Mater.* **2008**, *20*, 2044.
[12] Z. Li, Y. Gu, L. Wang, H. Ge, W. Wu, Q. Xia, C. Yuan, Y. Chen, B. Cui, R. S. Williams, *Nano Lett.* **2009**, *9*, 2306.
[13] J. Viheriala, T. Niemi, J. Kontio, T. Rytkonen, M. Pessa, *Electron. Lett.* **2007**, *43*, 150.
[14] S. Scheerlinck, P. Dubruel, P. Bienstman, E. Schacht, D. V. Thourhout, R. Baets, *J. Lightwave Technol.* **2009**, *27*, 1415.
[15] S. Scheerlinck, D. Taillaert, D. V. Thourhout, R. Baets, *Appl. Phys. Lett.* **2008**, *92*, 031104.
[16] G. Kostovski, D. J. White, A. Mitchell, M. W. Austin, P. R. Stoddart, *Biosens. Bioelectron.* **2009**, *24*, 1531.
[17] P. N. Minh, T. Ono, Y. Haga, K. Inoue, M. Sasaki, K. Hane, M. Esashi, *Opt. Rev.* **2003**, *10*, 150.
[18] M. Kim, K. Kim, N. Y. Lee, K. Shin, Y. S. Kim, *Chem. Commun.* **2007**, *22*, 2237.
[19] M. Aryal, F. Buyukserin, K. Mielczarek, X. M. Zhao, J. Gao, A. Zakhidov, W. Hu, *J. Vac. Sci. Technol. B* **2008**, *26*, 2562.
[20] H.-H. Wang, C.-Y. Liu, S.-B. Wu, N.-W. Liu, C.-Y. Peng, T.-H. Chan, C.-F. Hsu, J.-K. Wang, Y.-L. Wang, *Adv. Mater.* **2006**, *18*, 491.
[21] H. Kang, J. Lee, J. Park, H. H. Lee, *Nanotechnology* **2006**, *17*, 197.
[22] S. Jeon, J-U. Park, R. Cirelli, S. Yang, C. E. Heitzman, P. V. Braun, P. J. A. Kenis, J. A. Rogers, *Proc. Natl. Acad. Sci. USA.* **2004**, *101*, 12428.
[23] P. R. Stoddart, P. J. Cadusch, T. M. Boyce, R. M. Erasmus, J. D. Comins, *Nanotechnology* **2006**, *17*, 680.
[24] P. R. Stoddart, D. J. White, *Anal. Bioanal. Chem.* **2009**, *394*, 1761.
[25] D. J. White, A. P. Mazzolini, P. R. Stoddart, *J. Raman Spectrosc.* **2007**, *38*, 377.
[26] D. J. White, P. R. Stoddart, *Opt. Lett.* **2005**, *30*, 598.
[27] C. Viets, W. Hill, *J. Raman Spectrosc.* **2000**, *31*, 625.